

Synthesis, Characterization, and Polymerization Studies of Ethylenebis(hexamethylindenyl) Complexes of Zirconium and Hafnium

Paul Ransom, Andrew E. Ashley, N. David Brown, Amber L. Thompson, and Dermot O'Hare*

Chemistry Research Laboratory, Department of Chemistry, University of Oxford, Mansfield Road, Oxford, OX1 3TA, U.K.

Received October 15, 2010

The chemistry of a series of *ansa*-bridged ethylene-bis(hexamethylindenyl)zirconium and hafnium complexes has been explored. Treatment of $\text{EBI}^*\text{Li}_2\cdot\text{THF}_{0.38}$ with $\text{MCl}_4\cdot\text{THF}_2$ ($\text{M} = \text{Zr}, \text{Hf}$) gives *rac*- EBI^*MCl_2 (*rac*-**2**, *rac*-**3**) and *meso*- EBI^*MCl_2 (*meso*-**2**, *meso*-**3**) ($\text{M} = \text{Zr}$ and Hf), respectively. The *rac*- and *meso*- isomers can be separated by fractional crystallization. *meso*- $\text{EBI}^*\text{ZrMe}_2$ (*meso*-**4**) can be prepared by alkylation of *meso*-**2** with $\text{MeLi}\cdot\text{LiBr}$. The molecular structures of *rac*- and *meso*-**2** and *rac*- and *meso*-**3** have been determined by single-crystal X-ray crystallography. A comprehensive structural comparison between these compounds and related *ansa* metallocenes has been carried out. *rac*- and *meso*-**2** and *rac*- and *meso*-**3** in the presence of modified methylaluminoxane (MMAO) are very active catalyst precursors for the polymerization of ethene to give high-density polyethene (HDPE) with molecular weights (M_w) in the range 100 000–220 000 and polydispersities (M_w/M_n) of ca. 2.6. The activities of both catalyst precursors *rac*- and *meso*-**2** are some of the highest reported in the literature, at 61 800 and 38 200 $\text{kg PE/mol met/h/bar}$, respectively.

Introduction

Group 4 metallocenes are defined as pseudo-tetrahedral organometallic compounds in which the transition metal atom bears two η^5 -cyclopentadienyl-type ligands and two σ -ligands.¹ The introduction of an *ansa*-bridge into such species has led to many effects on the geometry, preventing mutual Cp ligand rotation and imposing rigidity and symmetry on the ligand framework, hence affecting the chemistry and reactivity of group 4 metallocenes, for example, increasing the electrophilicity of the metal.² The ring carbons of the π -ligands can bear numerous substituents, resulting in a high steric and electronic versatility via the ligands chosen. This has led to success in olefin polymerization catalysis due to the ability to manipulate activity, molecular weight, comonomer incorporation, and stereochemistry of the polymer produced by choice of Cp ring substituents, leading to rational catalyst design. The most studied *ansa*-metallocenes are the two-carbon bridged bis-indenyl zirconocenes.³ For example, in such species the introduction of alkyl substituents at various positions around the ring affects both the stereoregularity and the molecular weight of the polymer produced, together with the number of regioirregularities present.⁴ Each position on the indenyl ring when alkylated

can have a profound effect on the properties of the polymers produced.¹ We have previously reported the synthesis of the ethylene-bis(hexamethylindenyl) (EBI^*) ligand and the synthesis of *rac*- EBI^*Co .⁵ The synthesis of permethylated *ansa*-indenyl group 4 metallocenes has not been previously reported.

Results and Discussion

Synthesis and Characterization of *rac*- and *meso*- $\text{EBI}^*\text{ZrCl}_2$. The synthesis of $\text{EBI}^*\text{ZrCl}_2$ was attempted using a variety of EBI^* transfer and Zr-containing reagents in a number of different solvents and heating regimes. The most successful combination of reagents and conditions evolved from the treatment of $\text{ZrCl}_4\cdot\text{THF}_2$ with $\text{EBI}^*\text{Li}_2\cdot\text{THF}_{0.38}$ (**1**). Compound **1** was synthesized in a similar manner to EBI^*Na_2 ,⁵ using naphthalene and Li metal to effect the coupling of the fulvene moieties. Stirring **1** and $\text{ZrCl}_4\cdot\text{THF}_2$ in toluene at room temperature resulted in a 20% yield of $\text{EBI}^*\text{ZrCl}_2$ (**2**) (Figure 1).

After 15 h stirring at room temperature the crude reaction mixture comprises both *rac*- $\text{EBI}^*\text{ZrCl}_2$ (*rac*-**2**) and *meso*- $\text{EBI}^*\text{ZrCl}_2$ (*meso*-**2**). Aliquots were taken showing that stirring for a further 24 h had no impact on the isomer distribution. The two isomers show differences in their solubility properties, allowing their separation. *rac*-**2** is insoluble in most solvents, being moderately soluble in CH_2Cl_2 at room temperature and only slightly soluble in hot hexane. In contrast, *meso*-**2** is soluble in most common laboratory solvents. Similar results are found in the literature, with Zr and Hf *ansa*-bridged

*To whom correspondence should be addressed. E-mail: dermot.ohare@chem.ox.ac.uk. Tel: +44 (0) 1865 272686.

(1) Resconi, L.; Cavallo, L.; Fait, A.; Piemontesi, F. *Chem. Rev.* **2000**, 100, 1253–1346.

(2) Shapiro, P. J. *Coord. Chem. Rev.* **2002**, 231, 67–81.

(3) Chen, E. Y. X.; Rodriguez-Delgado, A.; Robert, H. C.; Mingos, D. M. P. In *Comprehensive Organometallic Chemistry III*; Elsevier: Oxford, 2007; pp 759–1004.

(4) Wang, B. *Coord. Chem. Rev.* **2006**, 250, 242–258.

(5) Ransom, P.; Ashley, A.; Thompson, A.; O'Hare, D. *J. Organomet. Chem.* **2009**, 694, 1059–1068.

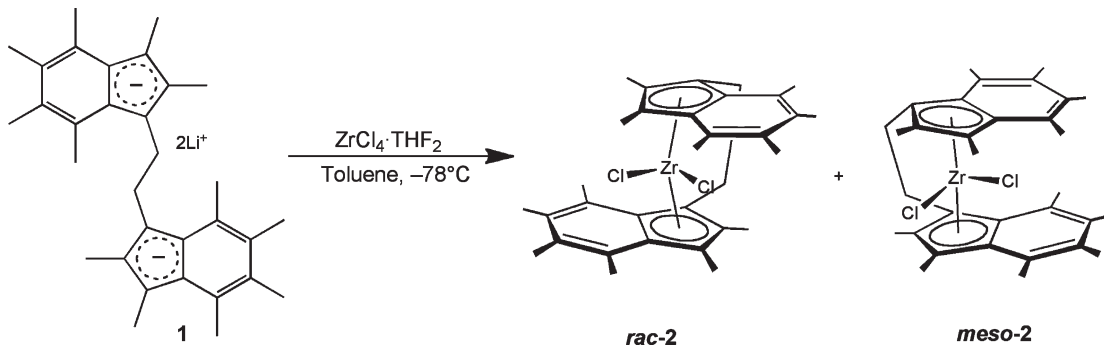


Figure 1. Synthesis of *rac*-2 and *meso*-2.

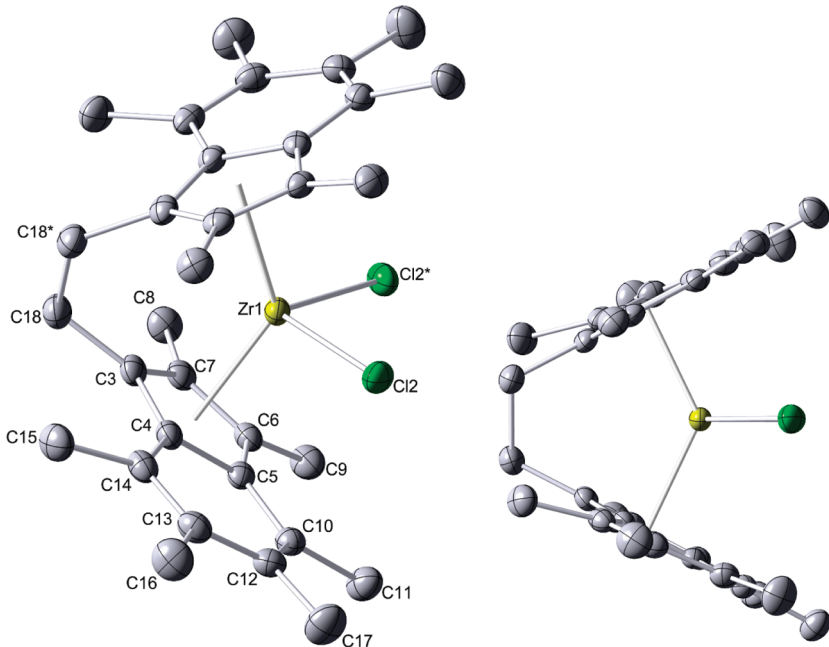


Figure 2. Molecular structure of *rac*-2, showing 50% probability ellipsoids. Hydrogen atoms have been omitted for clarity. Selected distances (\AA) and angles (deg): $Zr(1)-C(3) = 2.479(3)$, $Zr(1)-C(4) = 2.558(3)$, $Zr(1)-C(5) = 2.612(3)$, $Zr(1)-C(6) = 2.582(3)$, $Zr(1)-C(7) = 2.520(3)$, $Zr(1)-Cp_{cent} = 2.240$, $Zr(1)-Cl(2) = 2.4358(7)$, $\Delta_{M-C} = 0.054$, angle between C_6-C_5 planes = 2.6, $\delta = 129.4$, $Cl(2)-Zr-Cl(2) = 96.24(4)$, hinge angle = 2.7, $\alpha, \alpha' = 57.2, 55.6$, rotation angle = 124.4, $\beta, \beta' = -1.0, 0.3$.

bis-indenyl species having *rac* forms which are less soluble in organic solvents than their *meso* counterparts and being isolated by recrystallization.⁶ The solubility properties of *rac*-2 result in difficulties in its isolation and purification from the reaction residues and requires the use of repeated extractions or Soxhlet extraction.

Both isomers of **2** have been characterized by ¹H and ¹³C NMR spectroscopy, high-resolution mass spectrometry, elemental analysis, single-crystal X-ray diffraction, and electrochemical studies. Single crystals of *rac*-2 suitable for X-ray diffraction were grown as pale orange plates by the layering of a sample in CD_2Cl_2 with Et_2O . The compound crystallizes in the monoclinic space group $C2/c$, and a number of views are shown in Figure 2.

The complex is located on a crystallographic 2-fold axis of rotation; hence both indenyl rings are equivalent, and selected bond lengths and angles are given in Figure 2. The rotation angle (RA; Figure 3) is approximately 25° less than

that of *rac*-EBI*Co and *rac*-EBI*Fe,⁷ presumably due to the presence of the two Cl ligands hindering the movement of the indenyl rings into a more staggered conformation, caused by repulsion between $Cl(2)^*$ and $C(9)$. Analysis of the structure of the unbridged analogue Ind*₂ZrCl₂ reveals a RA of 98°, indicating a partially staggered arrangement of the Ind* rings. This is due to the steric requirements of the Ind* rings preventing a more eclipsed arrangement from that found in Ind₂ZrMe₂, which has a RA of approximately 10°.⁸ The presence of the ethylidene bridge in *rac*-2 prevents the twisting that would be required for a RA similarly approaching 100°. In addition, this RA of 124.4° in *rac*-2 results in an angle between the two Cl ligands and the Zr center of 96.24(4)°, significantly less than the ideal tetrahedral angle of 109.5°. The bond lengths of the Me groups to the EBI* ligand framework are similar to those in the Co and Fe species. This could again possibly be due to the presence of the Cl ligands preventing the EBI* framework from adopting a lowest energy twisted conformation,

(6) Nifant'ev, I. E.; Ivchenko, P. V. *Organometallics* **1997**, *16*, 713–715.

(7) Ransom, P. D. Ph.D. Thesis, University of Oxford, 2009.

(8) O'Hare, D.; Murphy, V.; Diamond, G. M.; Arnold, P.; Mountford, P. *Organometallics* **1994**, *13*, 4689–4694.

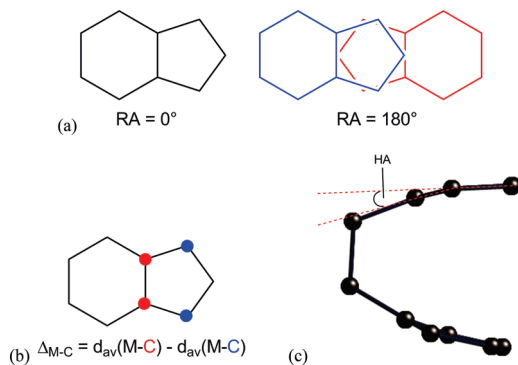


Figure 3. Schematic representation of the geometric parameters for indenyl metal complexes. (a) Rotation angle (RA) of indenyl ligand systems, showing fully eclipsed and fully staggered arrangements of the rings. (b) Calculation of the value of the slip parameter, Δ_{M-C} . (c) Side view of the *rac*-EBI* moiety with methyl groups and the upper aryl ring removed for clarity, showing the hinge angle (HA) formed on the lowering of the *ipso*-C out of the plane of the five-membered ring. A full definition of these terms is given in the SI.

which otherwise minimizes steric interactions between adjacent Me groups.

Electron-counting considerations make **2** an 16-valence electron species, which is supported by the low value of the slip parameter (Δ_{M-C} ; Figure 3), which indicates a bis- η^5 -bonding situation, and is the same as observed in the unbridged analogue Ind*₂ZrCl₂. It is slightly greater than that found in *rac*-EBI*Fe, and similarly the value found for Ind*₂ZrCl₂ is slightly greater than that for Ind*₂Fe.⁹ Furthermore, **2** shows a distinct alternation of bond lengths within the C₆ ring indicative of isolated double and single bonds, with the C₅ intra-ring distances being more similar as a result of the η^5 bonding and aromaticity. This results in a Zr–C_{Pcent} distance of 2.240 Å, similar to that found in Ind*₂ZrCl₂, with an average of 2.257 Å. Again, the bridged Zr species is comparable to its Fe analogue with similar values to those of the unbridged bis-Ind* compounds.

The presence of the two Cl ligands also has a significant effect on other structural parameters. As can be clearly seen in Figure 2, the two indenyl moieties are significantly bent away from the Zr center, with values of δ of 129.4° and α of 57.2°. The hinge angle (HA; Figure 3) is low; this may be attributed to both the presence of the Cl ligands and the η^5 -bonding mode. The structures of several other related Zr compounds have been reported in the literature, and parameters calculated from these are summarized in Table 1. It can be seen that the value of α for *rac*-EBI*ZrCl₂ is 2°–3° less than the other four *rac* species. This may reflect the permethylation of the ring periphery resulting in a stronger bonding interaction between the ligand and the Zr atom, pulling the rings together and lowering α . A trend of increasing RA can be seen on increasing the number of Me groups on the bridged indenyl moieties, supporting the earlier argument of steric interactions preventing **rac**-**2** from adopting a configuration more like its unbridged analogue Ind*₂ZrCl₂. Interestingly, the values of the HA for the three least methylated *rac* species are all negative; however, in the fourth case, where there is a Me group α to the bridge, and in **rac**-**2**, which also has a Me group α to the bridge,

it is positive. This could reflect the steric interactions between this Me group and the ethylenide bridge forcing the five-membered ring to bend out of the plane in the direction of the metal center to relieve these unfavorable interactions, thus resulting in a positive HA.

Interesting comparisons may be made between other species in Table 1. Looking at the effect the introduction of an *ansa*-bridge has upon Cp₂ZrCl₂ in the structure of {(C₅H₄)₂(CH₂)₂}ZrCl₂, it can be seen that α increases and δ decreases, as expected by the bridge enforcing a more pronounced bent sandwich geometry. The same trends are witnessed in the comparisons of Cp*₂ZrCl₂ with {(C₅Me₄)₂(CH₂)₂}ZrCl₂, Ind₂ZrCl₂, and EBI₂ZrCl₂; the value of α remains similar and δ decreases. With indenyl ligands the RA is also applicable and increases upon introduction of the *ansa*-bridge by 13° or 37° depending on the *meso*- or *rac*-isomer, respectively. The M–C_{Pcent} distance also depends on the conformation, decreasing in the *rac*-isomer and increasing in the *meso* form, possibly showing there to be a greater steric interaction between the indenyl moieties of EBI in the latter. In the permethylated case, introduction of the ethylenide bridge leads to an increase in α and a decrease in δ . One way the interactions are minimized is by the increase in the RA by nearly 36° in *rac*-**2** from that of Ind*₂ZrCl₂.

To investigate the effect of permethylation on the rings, the transition between the structures of Cp₂ZrCl₂ to Cp*₂ZrCl₂ and Ind₂ZrCl₂ to Ind*₂ZrCl₂ both show α to decrease and δ and M–C_{Pcent} to increase. This could therefore be due to the steric requirements of the Me ligands countering the increased metal–ligand bonding interaction upon permethylation of the ring periphery. This also becomes apparent in the comparison of Ind₂ZrCl₂ with Ind*₂ZrCl₂, in which the RA increases by over 52°, as the permethylated indenyl rings adopt a more staggered conformation to minimize Me steric interactions. When the two five-membered rings are connected with the ethylenide bridge, permethylation does not result in significant structural changes between {(C₅H₄)₂(CH₂)₂}ZrCl₂ and {(C₅Me₄)₂(CH₂)₂}ZrCl₂, perhaps due to the geometry being enforced by the *ansa* connection. However, in comparing *rac*-EBI₂ZrCl₂ with *rac*-**2**, significant differences are observed; α decreases, δ increases, and RA increases by 51°, despite both bonding in the *rac* form. This is similar to the effect seen upon permethylation in the unbridged analogues, the rings moving in an attempt to minimize unfavorable interactions between Me groups on the ring periphery.

X-ray quality crystals of *meso*-**2** were obtained as orange needles by the slow cooling of a concentrated hexane solution to –35 °C. The compound crystallizes in the triclinic space group P $\bar{1}$, with one EBI* moiety and one toluene molecule per asymmetric unit. Views of the molecular structure and relevant bond distances and angles are given Figure 5.

The *meso*-bonding mode of the EBI* ligand results in a RA of 46.8°, a value 25° greater than that found in [*meso*-EBI*Fe]⁺.⁷ This may be explained by the need to accommodate two halide ligands in the equatorial plane between the two planes of the indenyl rings, requiring a more staggered conformation in order to minimize ring Me–halide steric interactions. The slip parameter Δ_{M-C} is small, which indicates that the EBI* moiety is bound in an η^5 manner to the metal center. This is reflected in the bond alternation observed within the six-membered rings and aromatic-like bond length similarity within the five-membered rings. The average M–C_{Pcent} distance is 2.246 Å, which is statistically indistinguishable from that found in *rac*-**2**. Values of α and

(9) Westcott, S. A.; Kakkar, A. K.; Stringer, G.; Taylor, N. J.; Marder, T. B. *J. Organomet. Chem.* **1990**, 394, 777–794.

Table 1. Structural Parameters for Other Related Zr Compounds in the Literature

Compound	α	α' (°) ^a	δ (°) ^a	HA (°) ^a	RA (°) ^a	M-Cp _{cent} (Å)	Ref
Cp ₂ ZrCl ₂		52.3	129.3	-	-	2.199 2.201	50
Cp [*] ₂ ZrCl ₂		43.7	130.9	-	-	2.262	51
	57.4	60.1	125.2	-0.4 -5.4	-	2.180 2.183	52
	57.7	58.0	127.7	-0.5 -0.5	-	2.211 2.211	53
Ind ₂ ZrCl ₂		59.3	128.3		36.3	2.231 2.230	54
Ind [*] ₂ ZrCl ₂		44.3	138.3		88.6	2.255 2.259	8
	60.8	59.7	124.5	4.2 0.6	73.4	2.221 2.217	55
	59.7	59.6	109.9	-1.1 -1.3	49.6	2.230 2.223	56
	60.2	61.3	128.5	-1.8 -1.8	108.9	2.096 2.096	57
	60.5	60.9	125.2	-0.2 -1.5	48.3	2.213 2.220	58
	59.9	59.8	125.3	-0.4 -0.4	114.4	2.236 2.236	59
	62.4	60.2	123.8	6.3 3.8	37.4	2.224 2.223	59
	55.0	53.2	127.5	3.3	121.5	2.231	60
	57.2	55.6	129.4	2.7	124.4	2.240	This work
	56.9	54.4	128.7	6.0 3.3	46.8	2.244 2.248	This work

^a See Figures 3 and 4 and the SI for definitions of structural parameters.

δ are also very similar to those of **rac-2**. There is a notable increased twist at the C₆–C₅ ring junction similar to the value found in [meso-EBI*Fe]BF₄.⁷

With reference to Table 1, in the general case, it can be seen that while in the *rac* species the value of α seems to decrease on increasing the methylation of the ring periphery; in the *meso* species the opposite trend is observed. This may be explained by the increased sensitivity of the *meso* compounds to unfavorable interactions between the two indenyl rings, since they are held in a more eclipsed conformation. However, **meso-2** breaks this trend and actually has the lowest α value of all the *meso*-bonded species in Table 1. An increase in the value of α would be expected to correspond to a decrease in the angle δ .

The RA in **meso-2** also opposes the trend otherwise observed, being 9.4° greater than that of the dimethyl species. This is expected since increasing the steric bulk on the indenyl rings should favor an increase in the RA in order to minimize unfavorable steric interactions between them. The value of the HA for **meso-2** is similar to that of the dimethyl-substituted species in Table 1, and both show one of the indenyl rings to be more distorted than the other, as do their α values.

This may indicate that the distortion has its origins in the positioning of the Me groups on the aryl ring, adjacent to the C₆–C₅ ring junction.

Synthesis and Characterization of *rac*- and *meso*-EBI*HfCl₂, 3. The synthesis of **3** is detailed in Figure 6. It was accomplished using a similar procedure to that of the Zr analogue, although proceeding in higher yield. The reaction of **1** with HfCl₄·THF₂ in THF gave intractable products; however, if performed in toluene, it successfully produces a mixture of both *rac*- and *meso*-isomers. In contrast to its Zr analogue, **rac-3** does not suffer the same solubility problems and is soluble in C₆D₆ and hot hexane, although to a lesser extent than the *meso*-isomer. Hence, isomers are still easily separable by washing and crystallization.

Both isomers of **3** were characterized by ¹H and ¹³C NMR spectroscopy, mass spectrometry, elemental analysis, single-crystal X-ray diffraction, and electrochemical studies. The ¹H NMR spectral data of *rac*- and *meso*-**3** were similar to those observed with *rac*- and *meso*-**2**, in a number of different solvents. This implies the Zr and Hf species also have similar structures in solution.

Single crystals of **rac-3** suitable for X-ray diffraction were grown as pale yellow needles by the slow evaporation of a

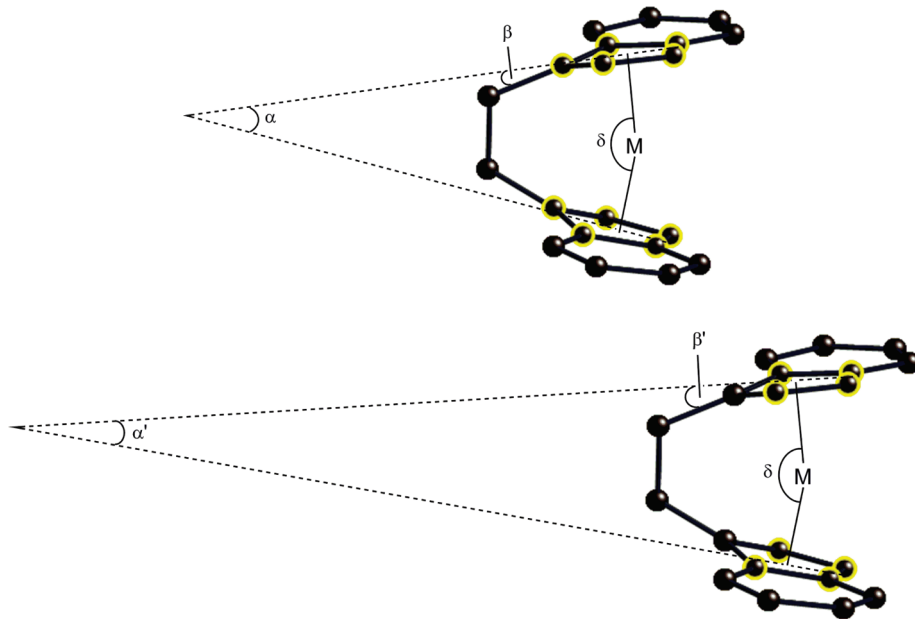


Figure 4. Schematic representation of the geometric parameters for EBI* compounds. α and β are formed as for Cp species from the best planes of the five-membered rings; α' and β' apply in the case of EBI*, in which the *ipso*-C lies out of the plane of the other four C atoms of the five-membered ring. A full definition of these terms is given in the SI.

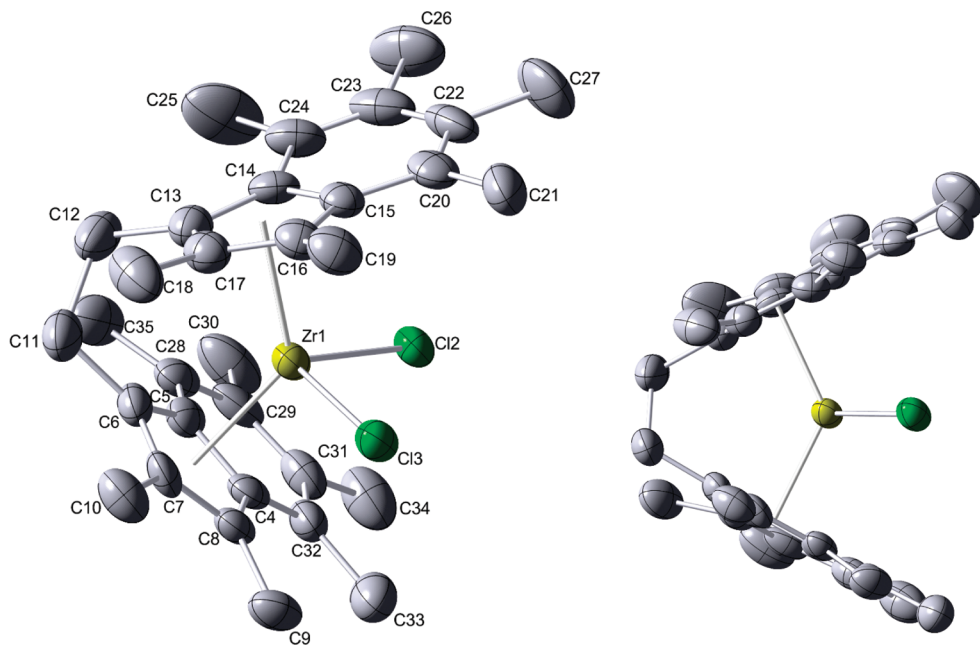


Figure 5. Molecular structure of *meso*-2, showing 50% probability ellipsoids. Hydrogen atoms have been omitted for clarity. Second view shows the location of the toluene molecule. Selected distances (\AA) and angles (deg): $\text{Zr}(1)-\text{C}(13) = 2.470(5)$, $\text{Zr}(1)-\text{C}(14) = 2.557(5)$, $\text{Zr}(1)-\text{C}(15) = 2.574(5)$, $\text{Zr}(1)-\text{C}(16) = 2.597(5)$, $\text{Zr}(1)-\text{C}(17) = 2.556(5)$, $\text{Zr}(1)-\text{Cp}_{\text{cent}} = 2.244 \text{\AA}$, $\text{Zr}(1)-\text{Cp}_{\text{cent}} = 2.248$, $\text{Zr}(1)-\text{Cl}(2) = 2.4276(13)$, $\text{Zr}(1)-\text{Cl}(3) = 2.4571(14)$, $\Delta_{\text{M}-\text{C}} = 0.033$, $\Delta_{\text{M}-\text{C}} = 0.083$, angle between C_6-C_5 planes = 6.4, 3.9, $\text{Cl}(2)-\text{Zr}-\text{Cl}(3) = 97.41(5)$, $\alpha, \alpha' = 56.9, 54.4$, $\beta, \beta' = 1.8, 3.2$, $\beta, \beta' = 1.3, 2.2$, $\delta = 128.7$, hinge angle = 6.0, 3.3, rotation angle = 46.8.

C_6D_6 solution. The molecule crystallizes on a special position in the monoclinic space group $C2/c$, with 0.5 EBI* moiety per asymmetric unit. Views of the molecular structure are shown in Figure 7. The structural parameters of *rac*-3 are very similar to those of the Zr analogue. The EBI* moiety bonds to the metal center in a similar bis- η^5 manner. In contrast with Zr, few structural examples of Hf-containing ethylidene-bridged species, or of Hf-containing indenyl com-

pounds, exist in the literature. Those that are found are shown in Table 2.

The slow cooling to -35°C of a concentrated toluene solution of *meso*-3 afforded pale yellow plates suitable for study by X-ray diffraction. The compound crystallizes in the monoclinic space group $P2_1/n$, with one EBI* moiety in the asymmetric unit. Views of the molecular structure are shown in Figure 8.

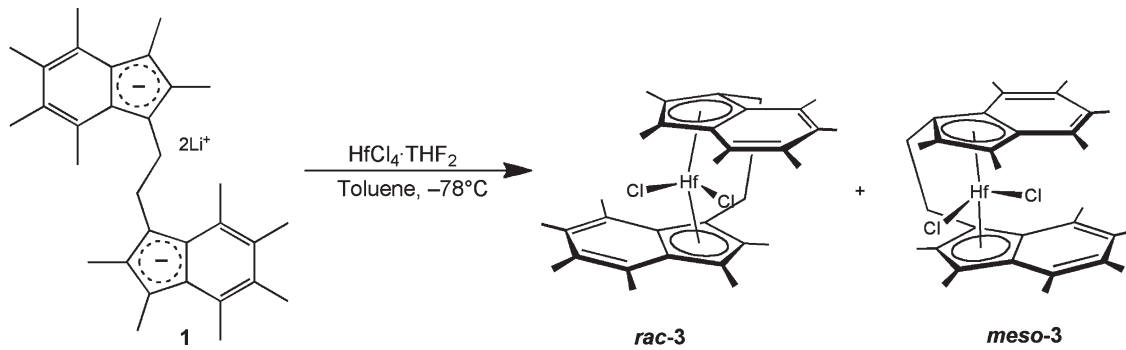


Figure 6. Synthesis of *rac*-3 and *meso*-3.

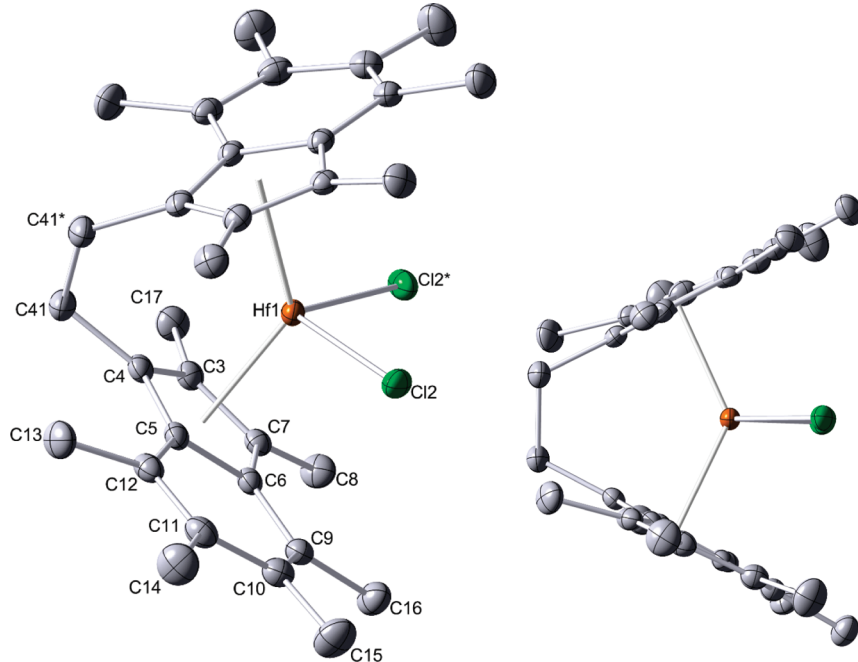


Figure 7. Molecular structure of *rac*-3 showing 50% probability ellipsoids. Hydrogen atoms have been omitted for clarity. Selected distances (\AA) and angles (deg): $\text{Hf}(1)-\text{C}(3) = 2.498(3)$, $\text{Hf}(1)-\text{C}(4) = 2.462(3)$, $\text{Hf}(1)-\text{C}(5) = 2.541(3)$, $\text{Hf}(1)-\text{C}(6) = 2.598(3)$, $\text{Hf}(1)-\text{C}(7) = 2.571(3)$, $\text{Hf}(1)-\text{C}_{\text{pcent}} = 2.222$, $\text{Hf}(1)-\text{Cl}(2) = 2.4118(7)$, $\Delta_{\text{M}-\text{C}} = 0.053$, angle between C_6-C_5 planes = 2.5, $\delta = 129.9$, $\text{Cl}(2)-\text{Hf}-\text{Cl}(2)^* = 95.43^\circ(4)$, hinge angle = 2.0, $\alpha, \alpha' = 57.0, 55.9$, rotation angle = 125.2, $\beta, \beta' = -1.0, 0.9$.

The value of the RA for *meso*-3 is similar to that found in *meso*-2, being just 1.8° less. The Hf–Cl bond lengths are not statistically distinguishable from those found in *meso*-2. Similarly, the Hf– C_{pcent} distance is not statistically distinguishable compared to the corresponding distance in *meso*-2. As demonstrated by the low values of $\Delta_{\text{M}-\text{C}}$, the EBI* moiety appears to bind in a bis- η^5 manner, as expected to afford an 18-valence-electron species. Again, this is confirmed by the bond length alternation in the C_6 ring and similarity in the C_5 ring.

As often appears to be the case (see Table 1 for examples), the value of α is slightly lower in the *meso* than *rac* form, and in a related manner a very small β parameter is found in the *meso* form and a low HA. However, in the case of EBI*, the parameter δ does not appear to be significantly affected by the specific bonding mode. Very few structural examples of unbridged indenyl-ligated Hf and none of *meso*-ligated Hf species exist in the literature, and so comparison with other compounds is difficult. With reference to Table 2, the value of α is higher and δ is lower compared with the analogous *syn* bis-indenyl compound.

Synthesis and Characterization of *rac*- and *meso*-EBI*ZrMe₂ (4). The synthesis of *rac/meso*-4 was carried out by the reaction of a slurry of *rac/meso*-2 at -78°C with either $\text{MeLi}\cdot\text{LiBr}$ or low-halide MeLi , shown in Figure 9. On formation of the Zr-Me species, solutions were observed to lighten in color from orange to yellow, becoming more soluble in all solvents tested. For example, *rac*-2 is only sparingly soluble in C_6D_6 ; however, *rac*-4 is completely soluble.

The *rac* form has a single methyl resonance at -0.99 ppm in C_6D_6 corresponding to six H atoms, consistent with literature data for *rac*-EBI ZrMe_2 , in which the Zr-Me resonance is observed as a singlet at -0.97 ppm.¹⁰ Only one singlet is observed due to the C_2 or *quasi* C_2 symmetry of the *rac* ligand framework, resulting in both Me ligands having the same environment. The NMR spectrum of *meso*-4 in C_6D_6 exhibits two singlets at -0.20 and -2.33 ppm, each corresponding to three H atoms. This compares well with values

(10) Balboni, D.; Camurati, I.; Prini, G.; Resconi, L.; Galli, S.; Mercandelli, P.; Sironi, A. *Inorg. Chem.* **2001**, *40*, 6588–6597.

Table 2. Structural Parameters of Related Hf-Containing Compounds in the Literature

Compound	α	α' (°) ^a	δ (°) ^a	HA (°) ^a	RA (°) ^a	M-Cp _{cent} (Å) ^a	Ref
	54.3		131.9	-	134.8	2.222 2.228	61,62
	52.5		131.4	-	59.4	2.218 2.225	61,62
	59.5	60.9	125.7	-2.6	106.4	2.198	63
	60.2	59.7	125.7	0.9	106.7	2.217	63
	57.0	55.9	129.9	2.0	125.2	2.222	This work
	56.9	55.1	129.9	4.2 2.6	45.0	2.226 2.225	This work

^aDefined in Figures 3 and 4 and the SI.

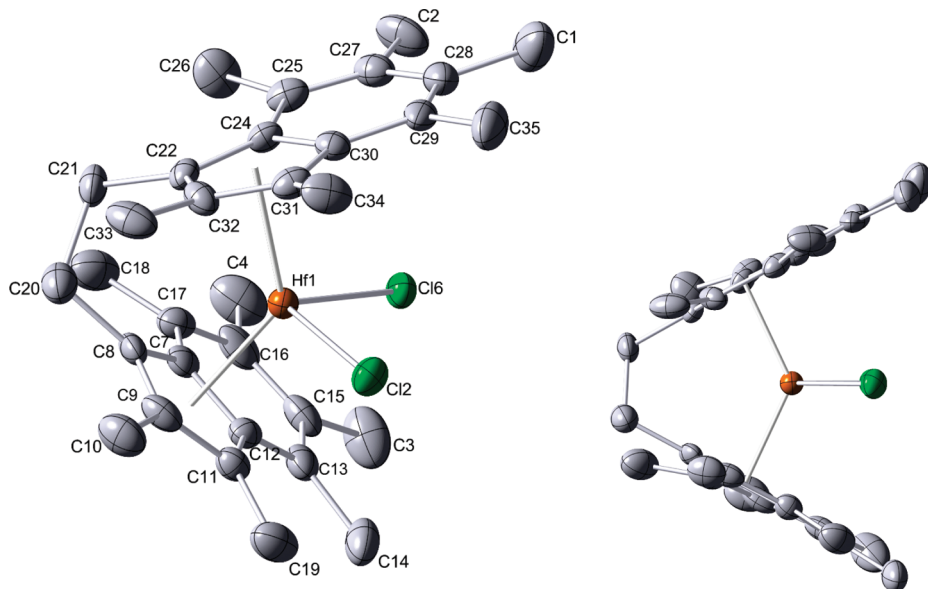


Figure 8. Molecular structure of **meso-3** showing 50% probability ellipsoids. Hydrogen atoms have been omitted for clarity. Selected distances (Å) and angles (deg): Hf(1)–C(7) = 2.562(6), Hf(1)–C(22) = 2.453(5), Hf(1)–C(8) = 2.459(5), Hf(1)–C(24) = 2.534(5), Hf(1)–C(9) = 2.478(6), Hf(1)–C(30) = 2.577(5), Hf(1)–C(11) = 2.553(5), Hf(1)–C(31) = 2.593(6), Hf(1)–C(12) = 2.622(5), Hf(1)–C(32) = 2.527(5), Hf(1)–Cp_{cent} = 2.225, Hf(1)–Cp_{cent} = 2.226, Hf(1)–Cl(2) = 2.4215(13), Hf(1)–Cl(6) = 2.3953(13), Δ_{M-C} = 0.086, Δ_{M-C} = 0.030, angle between C₆–C₅ planes = 1.5, 2.3, Cl(2)–Hf–Cl(6) = 96.02(5), α , α' = 56.9, 55.1, β , β' = 0.3, 0.4, 0.9, 1.9, δ = 129.9, hinge angle = 2.6, 4.2, rotation angle = 45.0.

for *meso*-EBIZrMe₂ of 0.12 and -2.20 ppm and *meso*-EBI-Me₂ZrMe₂ at -0.02 and -2.12 ppm,¹⁰ both species displaying

two singlets each. In the *meso* form, two singlets are observed since each Me group bound to the Zr center can be directed

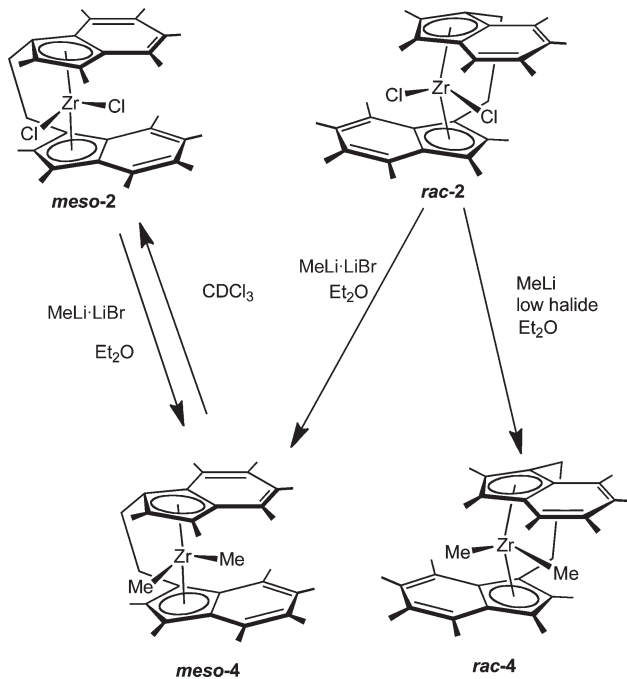


Figure 9. Reactions of *rac*- and *meso*-2 with low-halide MeLi and MeLi·LiBr and the observed interconversions.

either toward the six-membered rings or toward the five-membered rings, giving two distinct chemical environments. *rac/meso* distinction was also possible by analysis of the position and distribution of the ring-Me groups in the NMR spectrum; the second and third most upfield ring-Me peaks in the *rac* form have a chemical shift difference of 0.10 ppm, whereas in the *meso* form they are much closer together, with a difference of only 0.02 ppm.

The products obtained varied considerably with the choice of methylating reagent used. It was found that the reaction of pure *rac*-2 with low-halide MeLi gave, as expected, *rac*-4. However, if MeLi·LiBr was used with *rac*-2 in Et₂O, the product obtained was pure *meso*-4. The reaction of *meso*-2 with MeLi·LiBr first gave a mixture of *meso*-2 and a mixed Cl–Br ligated species and unidentified species with two Me resonances at –1.99 and –1.88 ppm, which upon addition of more MeLi·LiBr formed *meso*-4. Furthermore, an NMR sample of this solution of pure *meso*-4 in CDCl₃ was observed to convert over time to *meso*-2. Finally, addition of MeLi·LiBr to a mixture of *rac*-2 and *meso*-2 gave a mixture of *rac*- and *meso*-2 and 4 species as illustrated in Figure 9.

In the reaction of *meso*-2 with MeLi·LiBr, an initial unknown species with typical Zr-Me resonances in the NMR spectrum is observed. We suspect that the presence of LiBr leads to ligand exchange with Cl, forming the Br-containing species. Addition of further MeLi·LiBr to this mixture results in the exclusive formation of the dimethylated species *meso*-4. In C₆D₆, *meso*-4 is stable indefinitely. However in CDCl₃ *meso*-4 converts cleanly into *meso*-2 over several days at room temperature. No intermediates were observed in this reaction.

- (11) Bellemain-Lapponnaz, S.; Lo, M. M. C.; Peterson, T. H.; Allen, J. M.; Fu, G. C. *Organometallics* **2001**, *20*, 3453–3458.
- (12) Curnow, O. J.; Fern, G. M.; Hamilton, M. L.; Jenkins, E. M. *J. Organomet. Chem.* **2004**, *689*, 1897–1910.
- (13) Axtell, J. C.; Thai, S. D.; Morton, L. A.; Kassel, W. S.; Dougherty, W. G.; Zubris, D. L. *J. Organomet. Chem.* **2008**, *693*, 3741–3750.

The *rac/meso* isomerization of metallocenes has been reported in the literature,^{11–13} together with that of *ansa*-bridged species.^{14–19} In order for isomerizations to occur, one of the Cp moieties must dissociate from the metal and recoordinate by the other face. Interchange is promoted by coordinating solvents and LiCl, and mechanisms have been proposed involving the coordination of anions and/or donor solvents to the metal center with cation assistance to encourage the M–Cp bond heterolysis.¹⁷ Other mechanisms have also been identified, including photochemical or thermal homolysis, heteroatom-assisted enantioface exchange, and silatropic rearrangement.¹⁹ In *ansa*-indenyl systems, the *rac* form has been noted as being more stable due to the steric crowding in the *meso* form between the π-bonded ligands and the two six-membered rings. In addition, the *meso*-isomer is open to nucleophilic attack due to one lateral coordination site being relatively open, leading to a *meso* to *rac* isomerization and the thermodynamic product.²⁰ A patent application exists stating that the *meso* form of metallocenes can be catalytically isomerized to the *rac* form by heating either the pure *meso* or a *rac/meso* mixture with a group 1 or group 2 metal halide in an organic solvent.²¹ Similarly, another patent notes metal alkoxides isomerize kinetic EBI {EBI = ethylenebis(indenyl)} to thermodynamic EBI and *meso*-EBITMS {EBITMS = ethylenebis(indenyl)tetramethylsilane} to *rac*-EBITMS.²² This is summarized in a recent study, which concludes that Cp ligands are easily displaced from zirconocene species by Cl[–] under mild conditions, and facile loss of metallocene stereochemistry can occur under conditions where free Cl[–] or other nucleophilic species are present.¹⁹

Although the literature studies mentioned detailed *rac/meso* isomerization between species with the same σ-bonded ligands, Figure 9 shows a conversion between *rac*-2 and *meso*-4 species upon reaction with MeLi·LiBr. Since using low-halide MeLi results in the formation of *rac*-4, a proposed mechanism again involves the presence of LiBr in the former system or Cl[–] from the LiCl generated upon ligand exchange, perhaps leading to Zr–Cp bond homolysis before or after the methylation step and resulting in an effective *rac* to *meso* isomerization. The reasons that this isomerization leads to what has previously been considered in the literature to be the least thermodynamically favored *meso* form and not the usual *meso* to *rac* isomerization are unclear; however, it is possible that permethylation of the ring periphery results in the *meso* form no longer being the more sterically energetically unfavorable of the two.

- (14) Haar, C. M.; Stern, C. L.; Marks, T. J. *Organometallics* **1996**, *15*, 1765–1784.
- (15) Giardello, M. A.; Conticello, V. P.; Brard, L.; Sabat, M.; Rheingold, A. L.; Stern, C. L.; Marks, T. J. *J. Am. Chem. Soc.* **1994**, *116*, 10212–10240.
- (16) Hultzsch, K. C.; Spaniol, T. P.; Okuda, J. *Organometallics* **1997**, *16*, 4845–4856.
- (17) Yoder, J. C.; Day, M. W.; Bercaw, J. E. *Organometallics* **1998**, *17*, 4946–4958.
- (18) Amako, M.; Schinkel, J.; Brook, M. A.; McGlinchey, M. J.; Britten, J. F. *Organometallics* **2005**, *24*, 1533–1543.
- (19) Buck, R. M.; Vinayavekhin, N.; Jordan, R. F. *J. Am. Chem. Soc.* **2007**, *129*, 3468–3469.
- (20) Diamond, G. M.; Jordan, R. F.; Petersen, J. L. *J. Am. Chem. Soc.* **1996**, *118*, 8024–8033.
- (21) Lin, R. W. (Albemarle Corporation, USA). Patent Application: US, 1999.
- (22) Gately, D. A. (Boulder Scientific Company, USA). Patent Application: WO, 2000.

Electrochemical Studies. The electrochemical properties of *rac*- and *meso*-**2/3** were studied as solutions in CH_2Cl_2 with $0.1 \text{ mol}^{-1} [\text{N}^n\text{Bu}_4]\text{PF}_6$ as supporting electrolyte. All data were recorded at room temperature under scan rates of 50/100/200 mV s^{-1} and referenced internally to the $\text{Cp}_2\text{Fe}/\text{Cp}_2\text{Fe}^+$ couple at +0.46 V vs SCE under identical conditions.²³ Examples of the cyclic voltammograms obtained for *rac*-**2** are shown in Figure 10. Two electrochemical events are seen, at -0.45 and +0.86 V vs SCE. The reduction at -0.45 V can be seen to be irreversible at all scan rates; however, the oxidation at +0.86 V appears to become less irreversible on the electrochemical time scale at higher scan rates. In the case of *meso*-**2**, shown in Figure 11, again an oxidation event and a reduction event are witnessed, at slightly different values of -0.38 and +0.85 V vs SCE, respectively. However, the oxidation appears to be irreversible at all scan rates employed. These data, together with those of other selected bent Zr metallocene dichloride species, are summarized in Table 3.

The literature reduction potentials quoted in Table 3 are given as reversible; however, the oxidation potentials are reported to be irreversible. Other such studies have indicated that the one-electron reduction of $\text{Cp}^{\text{R}}_2\text{ZrCl}_2$ giving $[\text{Cp}^{\text{R}}_2\text{ZrCl}_2]^-$ is often reversible, although it has also been noted that increasing substitution of the Cp rings reduces the reversibility.²⁴ The reduction and oxidation potentials have been discussed in the literature with relation to the energies of the frontier orbitals, the LUMO and HOMO, respectively.²⁵ The irreversible reduction potentials observed for *rac*- and *meso*-**2** are significantly less negative than those of the other species in Table 3, and the oxidation is significantly less positive. The less positive oxidation potential could imply that the species is easier to oxidize due to a higher energy HOMO. Alternatively, the seemingly vastly different values of E_{red} and E_{ox} for **2** may indicate decomposition of the compounds, for example by loss of Cl^- ligands, which would also account for their irreversibility.

Electrochemical studies on *rac*- and *meso*-**3** gave very similar results to the Zr analogues; two processes in the CV trace were observed: an irreversible reduction and an irreversible oxidation. Unlike the Zr analogue, the oxidation of the *rac*-isomer appeared to be irreversible at all scan rates employed; however, the *meso* form showed a very slight decrease in irreversibility at a scan rate of 200 mV s^{-1} , although not as significantly as that of *rac*-**2**. These data are summarized together with those of Cp_2HfCl_2 , the only related Hf species for which electrochemical data are available in the literature in Table 4. Upon comparison of Table 3 and Table 4, it can be seen that similar values are obtained for the Zr and Hf EBI* species. There is a negative shift in values of E_{red} and E_{ox} upon progressing from Cp_2ZrCl_2 to Cp_2HfCl_2 , and although this is seen in E_{red} for the *rac*-EBI* species, it does not appear to be the case with E_{ox} or for the *meso* forms. Again, the oxidation and reduction potentials for *rac*- and *meso*-**3** are greatly different from what might be expected upon comparison with Cp_2HfCl_2 and extrapolation from the Zr species in Table 3, perhaps suggesting the CV trace shows sample decomposition and not the formation of $[\text{EBI}^*\text{HfCl}_2]^{\pm}$ species.

(23) Connelly, N. G.; Geiger, W. E. *Chem. Rev.* **1996**, *96*, 877–910.

(24) Langmaier, J.; Samec, Z.; Varga, V.; Horáček, M.; Choukroun, R.; Mach, K. *J. Organomet. Chem.* **1999**, *584*, 323–328.

(25) Loukova, G. V. *Chem. Phys. Lett.* **2002**, *353*, 244–252.

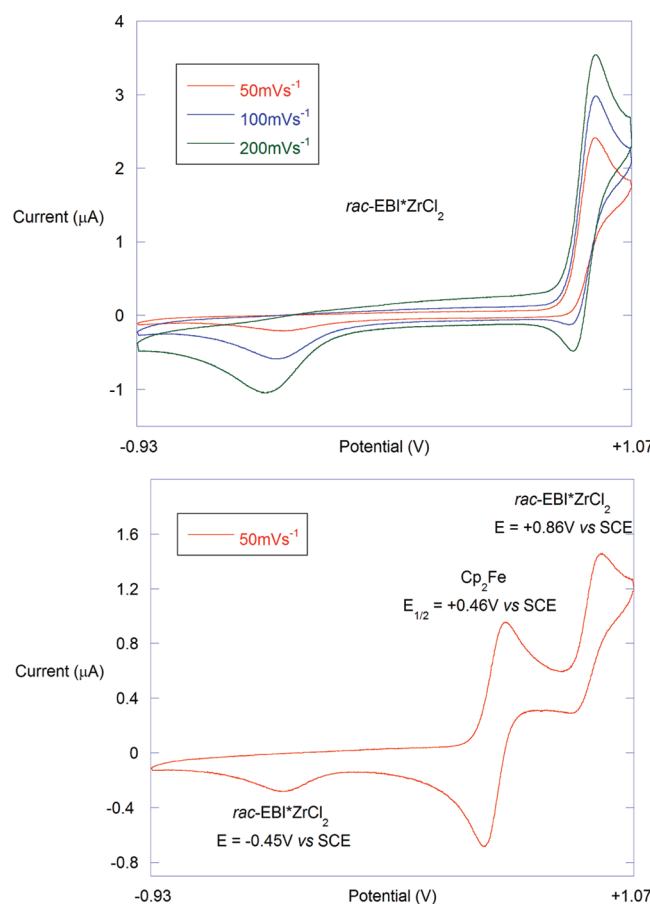


Figure 10. Cyclic voltammograms in CH_2Cl_2 of *rac*-**2** (top) and *rac*-**2** with internal Cp_2Fe reference (bottom). Potentials were determined by square-wave voltammetry and are given vs SCE.

OLEFIN POLYMERIZATION STUDIES. Both *rac* and *meso* forms of **2** and **3** were tested for their ability to act as catalyst precursors for ethene polymerization in the presence of the activator-modified methylaluminoxane (MMAO-3A, Akzo Nobel). The reactions were performed under 10 bar of ethene pressure in a 5 L batch reactor, with the pro-catalysts dissolved in toluene with half the MMAO activator added in this solution (5000 equivalents vs metal) and the other half added in the 5 L steel autoclaves. The polymerization conditions and results are summarized in Table 5.

Both *rac*-**2** and *meso*-**2** are very active for ethene polymerization, with catalytic activities obtained between 3×10^7 and $6 \times 10^7 \text{ gPE/mol Zr/h/bar}$. For both the *rac* and *meso* forms the Hf compounds are an order of magnitude less active than the Zr analogues. In the case of **2**, the *rac* isomer was approximately twice as active as the *meso*; this trend is reversed in **3**, with the *meso* form being over twice as active as the *rac*. Comparative studies on the catalytic performance of other group 4 metallocene compounds generally agree with the activity of Zr complexes being substantially higher than that of the corresponding Hf compounds under similar conditions.^{26–28} Studies have been performed on the electronic and steric effects of the ligands, together with the

(26) Weiss, K.; Neugebauer, U.; Blau, S.; Lang, H. *J. Organomet. Chem.* **1996**, *520*, 171–179.

(27) Jany, G.; Gustafsson, M.; Repo, T.; Aitola, E.; Dobado, J. A.; Klinga, M.; Leskela, M. *J. Organomet. Chem.* **1998**, *553*, 173–178.

(28) Alt, H. G.; Fottinger, K.; Milius, W. *J. Organomet. Chem.* **1998**, *564*, 109–114.

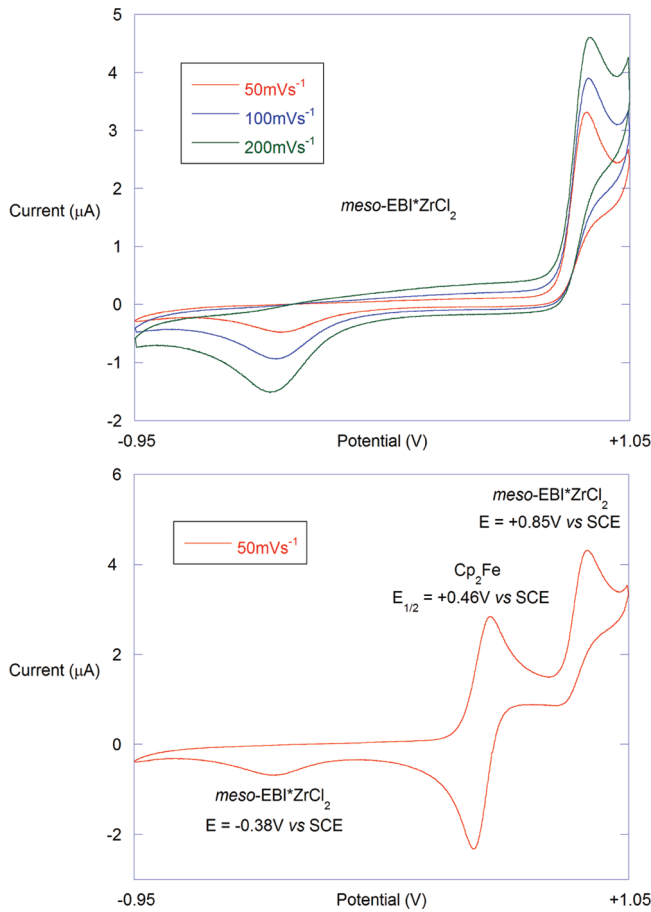


Figure 11. Cyclic voltammograms in CH_2Cl_2 of *meso*-**3** (top) and *meso*-**3** with internal Cp_2Fe reference (bottom). Potentials were determined by square-wave voltammetry and are given vs SCE.

Table 3. Oxidation and Reduction Potentials for Selected Bent Zr Metallocenes

compound	E_{red} (V vs SCE)	E_{ox} (V vs SCE)	ref
Cp_2ZrCl_2	-1.63	+1.86	64
$Cp^*_2ZrCl_2$	-1.94	not reported	52
$\{(C_5H_4)_2(CH_2)_2\}ZrCl_2$	-1.72	not reported	52
Ind_2ZrCl_2	-1.59	+1.48	64
$EBIZrCl_2$	-1.57	+1.36	64
rac - 2	-0.45	+0.86	this work
meso - 2	-0.38	+0.85	this work

polymerization conditions, on the ethylene polymerization activities of zirconocene catalysts.^{29–32} The role of the aluminoxane cocatalyst has been examined, and for most homogeneous metallocene catalysts a large excess of aluminoxane is required for the polymerization to achieve its optimum productivity. The literature commonly reports Al/Zr ratios between 1000 and 50 000, with activity generally increasing as the ratio increases, up to an optimal value. It is therefore important when comparing activity data to compare similar

(29) Janiak, C.; Versteeg, U.; Lange, K. C. H.; Weimann, R.; Hahn, E. *J. Organomet. Chem.* **1995**, *501*, 219–234.

(30) Möhring, P. C.; Coville, N. J. *Coord. Chem. Rev.* **2006**, *250*, 18–35.

(31) Kaminsky, W.; Engehausen, R.; Zoumis, K.; Spaleck, W.; Rohrmann, J. *Makromol. Chem.* **1992**, *193*, 1643–1651.

(32) Tian, J.; Huang, B. *Macromol. Rapid Commun.* **1994**, *15*, 923–928.

Table 4. Oxidation and Reduction Potentials for **4 and Cp_2HfCl_2**

compound	E_{red} (V vs SCE)	E_{ox} (V vs SCE)	ref
Cp_2HfCl_2	-1.93	+1.81	64
rac - 4	-0.57	+0.87	this work
meso - 4	-0.36	+0.86	this work

conditions and Al/Zr ratios where possible. MAO is the most commonly used aluminoxane; however, it has been shown that MMAO/metallocene and MAO/metallocene systems have comparable polymerization rates; hence values in this work can be readily compared with the literature.³³

The effect of ligand substitution on the polymerization activity has been rationalized on steric grounds, with unsubstituted zirconocene dichloride being more active than mixed sandwiches, which are in turn more active than symmetrically substituted compounds, as shown in the upper section of Table 6. The Me groups have a sterically hindering effect and decrease the flexibility toward the spatial requirements of the incoming monomer and the growing polymer chain. It can also be seen from Table 6 that although the Al/Zr ratio is slightly higher for the **2** samples, the activity is significantly greater than for all the Cp -based Zr systems. The data in the lower half of Table 6 show that the unbridged Ind species Ind_2ZrCl_2 is approximately 9 times more active than Cp_2ZrCl_2 . Furthermore, they indicate that the introduction of an *ansa* bridge in this Ind case reduces the activity of the resulting catalyst by almost 7 times to a value similar to that of Cp_2ZrCl_2 . These trends of decreasing activity with increasing steric substitution, and decreased activity of bridged compared with nonbridged species, have also been documented elsewhere in the literature.³⁴

The data in Table 6 suggest that, even though information at equivalent Al/Zr ratios is not available, the EBI* $ZrCl_2$ catalysts are much more active than either the Cp -based, unbridged Ind, or *ansa* Zr species given. It appears that the EBI* ligand array counters the usual trends, being both *ansa*-bridged and fully substituted yet also highly active. This may be due to electronic factors impacting catalyst activity beyond a certain steric threshold.³⁰ It has been reported that decreasing electron density at the metal center reduces rates of propagation and chain transfer in ethene polymerization. The effect of the former is more pronounced, leading to a decrease in activity and polymer molecular weights with electron-deficient catalysts.³⁵ Therefore, the high activity of the EBI* catalysts reflects the highly electron donating capacity of the ligand, outweighing negative steric effects. This has also been observed through the high activity in ethylene polymerization of the sterically congested and substituted metallocene species (Me_2Si)($IndMe_3$) $_2ZrCl_2$, due to electronic effects in the insertion reaction.³⁶ As mentioned earlier, experimentally determined values of catalyst activity are highly dependent upon the precise reaction conditions, and often the kinetic profile or lifetime of the catalyst is not mentioned. However, to enable comparison of values in the literature, Gibson suggests converting activity figures to g_{polymer}/mmol metal/h/bar and placing the catalyst on a scale of merit ranging from very low to very high. On this

(33) Hamielec, A. E.; Soares, J. B. P. *Prog. Polym. Sci.* **1996**, *21*, 651.

(34) Silveira, F.; Simplicio, L. M. T.; Novais da Rocha, Z.; Zimnoch dos Santos, J. H. *Appl. Catal., A* **2008**, *344*, 98–106.

(35) Lee, I. M.; Gauthier, W. J.; Ball, J. M.; Iyengar, B.; Collins, S. *Organometallics* **1992**, *11*, 2115–22.

(36) Kaminsky, W. *J. Chem. Soc., Dalton Trans.* **1998**, 1413–1418.

Table 5. Summary of Ethylene Polymerization with *rac*- and *meso*-EBI^{*}MCl₂ (M = Zr, Hf)^a

catalyst	catalyst amount	MMAO	run time	polymer yield (g)	productivity (g _{PE} /mol met/h)
<i>rac</i>-2	1.17 mg, 2 μmol Zr	20 mmol, 10 000 equiv/Zr	15 min	309	6.18×10^8
<i>meso</i>-2	1.17 mg, 2 μmol Zr	20 mmol, 10 000 equiv/Zr	30 min	382	3.83×10^8
<i>rac</i>-3	1.35 mg, 2 μmol Hf	20 mmol, 10 000 equiv/Hf	60 min	25	1.25×10^7
<i>meso</i>-3	1.35 mg, 2 μmol Hf	20 mmol, 10 000 equiv/Hf	60 min	67	3.35×10^7

^a Polymerization conditions: 1.8 L of isobutene, 70 °C, P_{C2} = 10 bar.

Table 6. Summary of Ethene Polymerization Activity for MAO-Activated Zirconocenes Compared to Related EBI^{*} Compounds

catalyst	activity (kg _{PE} /g _{Zr} /h/bar)	Al/Zr ratio	ref
Cp ₂ ZrCl ₂	100	8000:1	29 ^a
(CpMe ₄ H)CpZrCl ₂	51	8000:1	29 ^a
Cp [*] CpZrCl ₂	34	8000:1	29 ^a
(CpMe ₄ H) ₂ ZrCl ₂	27	8000:1	29 ^a
Cp [*] ₂ ZrCl ₂	27	8000:1	29 ^a
<i>rac</i>-2	677	10000:1	this work ^b
<i>meso</i>-2	419	10000:1	this work ^b
Cp ₂ ZrCl ₂	37	4000:1	29 ^a
Cp [*] ₂ ZrCl ₂	19	4000:1	29 ^a
Ind ₂ ZrCl ₂	343	5000:1	27 ^c
<i>rac</i>-EBIZrCl₂	51	5000:1	27 ^c

^a 70 °C, P_{C2} = 5 bar. ^b 70 °C, P_{C2} = 10 bar. ^c 50 °C, P_{C2} = 2 bar.

scale ***rac*-2**, ***meso*-2**, ***rac*-3**, and ***meso*-3** are some of most active reported metallocene catalyst precursors (Table 6).³⁷

Samples of each polymer produced by EBI^{*}MCl₂ (M = Zr, Hf)-based catalysts were analyzed by differential scanning calorimetry (DSC) in order to determine their melting points, and values obtained are shown in Table 7. Each of the four polyethylene samples analyzed have a similar melting point. For comparison, the literature reports that polyethylene synthesized by *meso*-EBIZrCl₂ catalyst has a melting point determined by DSC of 123 °C, compared with 135 °C for that of the *rac* analogue.^{38,39} This reduction in melting point has been attributed to the introduction of short branches into the polyethylene chain and the formation of linear low-density polyethylene (LLDPE). However, a number of other polyethylene samples produced via *ansa*-bridged substituted *meso* zirconocene catalysis show a melting point of approximately 133 °C.⁴⁰ The polyethylene samples are comparable with those in the literature for nonbranched, linear high-density polyethylene (HDPE).⁴¹

The polyethylene samples all have similar molecular weight distributions; however the sample produced by the ***meso*-3** catalyst is of considerably lower molecular weight (approximately half) and has the broadest distribution (Table 8). Within the other three samples, there are small but clear differences; the polymer produced with ***rac*-3** as catalyst has the highest weight average molecular weight (*M*_w) and broadest distribution, while that from ***meso*-2** has the lowest *M*_w. Although the *M*_w and *M*_n of the Zr-catalyzed samples

(37) Britovsek, G. J. P.; Gibson, V. C.; Wass, D. F. *Angew. Chem., Int. Ed.* **1999**, *38*, 428–447.

(38) Izzo, L.; Caporaso, L.; Senatore, G.; Oliva, L. *Macromolecules* **1999**, *32*, 6913–6916.

(39) Chien, J. C. W.; He, D. *J. Polym. Sci., Part A: Polym. Chem.* **1991**, *29*, 1585–1593.

(40) Melillo, G.; Izzo, L.; Zinna, M.; Tedesco, C.; Oliva, L. *Macromolecules* **2002**, *35*, 9256–9261.

(41) Leino, R.; Lutikkhedde, H. J. G.; Lehmus, P.; Wilen, C.-E.; Sjoeholm, R.; Lehtonen, A.; Seppaelae, J. V.; Naesman, J. H. *Macromolecules* **1997**, *30*, 3477–3483.

Table 7. Melting Points of Polyethylene Samples

catalyst	melting point of polyethylene ^a produced (±0.03 °C)
<i>rac</i>-2	133.16
<i>meso</i>-2	133.75
<i>rac</i>-3	134.59
<i>meso</i>-3	132.03

^a Measured by DSC.

Table 8. Molecular Weight Averages and Polydispersities (*M*_w/*M*_n)^a

catalyst	technique	<i>M</i> _w	<i>M</i> _n	<i>M</i> _w / <i>M</i> _n
<i>rac</i>-2	GPC	215 000	88 800	2.4
	GPC	215 000	91 200	2.4
	GPC–viscosity	217 000	83 200	2.6
	GPC–viscosity	216 000	85 000	2.5
<i>meso</i>-2	GPC	203 000	86 100	2.4
	GPC	203 000	86 400	2.4
	GPC–viscosity	202 000	80 000	2.5
	GPC–viscosity	202 000	79 900	2.5
<i>rac</i>-3	GPC	228 000	85 600	2.7
	GPC	227 000	85 100	2.7
	GPC–viscosity	228 000	79 800	2.9
	GPC–viscosity	225 000	77 700	2.9
<i>meso</i>-3	GPC	106 000	33 700	3.2
	GPC	107 000	34 800	3.1
	GPC–viscosity	103 000	34 200	3.0
	GPC–viscosity	103 000	35 200	2.9

^a Data obtained by high-temperature GPC and combined GPC–viscosity, with duplicate runs performed for each sample. Conditions: 15 mg of sample dissolved in 15 mL of 1,2,4-trichlorobenzene (with antioxidant), 190 °C, refractive index and differential pressure (for GPC–viscosity) detector.

are different, their polydispersities are identical. Within Hf-catalyzed samples, a similar effect is observed in polydispersities. It appears that for both Zr- and Hf-catalyzed polyethylene samples the polymers with the highest *M*_w are those of the *rac* rather than the *meso* catalysts. From Table 7 and Table 8 it can be seen that there exists a correlation between the highest values of *M*_w, *M*_n, and melting point for the *rac*-3-catalyzed polymer and the lowest values of *M*_w, *M*_n, and melting point for the resultant *meso*-3 polyethylene.

It has been noted in the literature that molecular weight distributions of polymers obtained in ethylene polymerization studies vary with the reaction conditions, making direct quantitative comparisons between previously published results difficult.^{41,42} However, values of *M*_w and polydispersity of EBI^{*}MCl₂-catalyzed polymers are similar to those found in the literature.^{31,32,42} Some reported values of activity, *M*_w, and polydispersity for a number of metallocene-catalyzed polyethylene samples are given in Table 9.

(42) D'Agnillo, L.; Soares, J. B. P.; Penlidis, A. *Macromol. Chem. Phys.* **1998**, *199*, 955–962.

Table 9. Comparison of Activity, M_w , and Polydispersity (M_w/M_n) for Select Zr and Hf Ind Catalysts in Ethylene Polymerization

catalyst	activity (kg _{PE} /mol met/h/bar)	Al/Zr ratio	M_w ($\times 10^3$)	M_w/M_n	ref
Ind ₂ ZrCl ₂	31 250	5000:1	490	2.3	27 ^a
Ind ₂ HfCl ₂	3906	5000:1	959	2.6	27 ^a
<i>rac</i> -EBIZrCl ₂	4688	5000:1	240	3.2	27 ^a
<i>rac</i> -EBIHfCl ₂	1050	5000:1	387	4.4	27 ^a
<i>rac</i> -EBIOSiZrCl ₂	840	10 000:1	200	3.2	41 ^b
<i>rac</i> -EBIOSiHfCl ₂	80	10 000:1	280	3.3	41 ^b
<i>rac</i> -EBTHIOSiZrCl ₂	1000	10 000:1	>1000	2–4	41 ^b
<i>rac</i>-2	61 800	10 000:1	217	2.6	this work ^c
<i>meso</i>-2	38 200	10 000:1	202	2.5	this work ^c
<i>rac</i>-3	1250	10 000:1	227	2.9	this work ^c
<i>meso</i>-3	3350	10 000:1	103	3.0	this work ^c

^a 50 °C, P_{C_2} = 2 bar. ^b 40 °C, P_{C_2} = 2.5 bar, IOSi = 2-OSiMe₂^tBu-indenyl. ^c 70 °C, P_{C_2} = 10 bar.

In general, Hf catalysts are less active than their Zr analogues, and polymers obtained with Hf catalysts show a higher molecular weight than the corresponding Zr species under similar conditions.^{26–28} However, ***meso*-3** seems unusual in this regard in that it has a dramatically lower M_w . The data in Table 9 show that the *ansa*-bridged Ind species produce polymers with much lower M_w than the unbridged analogues. The values of M_w for the polymers produced by *rac*-EBIZrCl₂ and ***rac*-2** are similar; however, the M_w of the ***rac*-3**-catalyzed sample is also lower than anticipated, despite being greater than its Zr-catalyzed analogue. It has been found that changing the catalyst type dramatically affects the M_w , with M_w values increasing in the order EBI^{*}ZrCl₂ < Cp₂ZrCl₂ < Cp₂HfCl₂ < Cp₂TiCl₂ < EBTHIZrCl₂.⁴² Furthermore, the same study found increases in MAO concentrations to decrease average molecular weight. It is not unexpected therefore that the M_w values for the EBI^{*} species studied are the lowest in Table 9. These differences are usually explained by different ratios of propagation rates to chain termination transfer rates among the catalysts. As mentioned earlier, decreasing electron density at the metal center reduces both these rates, but the propagation rate decreases to a greater extent, leading to a decrease in polymer molecular weights with electron-deficient catalysts. This is in contrast to that observed with EBI^{*}-catalyzed polyethylene samples. The GPC–viscosity data indicate little, if any, difference in terms of the long chain branching between the four samples and between the four samples and the known linear polyethylene. The GPC–viscosity data, together with the melting point data, strongly suggest that all samples produced by the EBI^{*}MCl₂ (M = Zr, Hf) catalytic precursors are HDPE.

Both ***rac*-2** and ***rac*-3** were found to be inactive for the polymerization of propene upon treatment with MMAO in either toluene, hexane, or liquid propene. It seems that the Me groups on the indenyl moieties in ***rac*-2** and ***rac*-3** result in the compounds being too sterically hindered to allow propylene insertion into the M–C bond.

Concluding Remarks

Several group 4 transition metal complexes of the EBI^{*} ligand have been synthesized and characterized. Both *rac* and *meso* forms of Zr and Hf dihalide species have been structurally characterized and compared with literature compounds when possible. Alkyl Zr and Hf derivatives have been formed, and *rac/meso* isomerization of the Zr species has been observed. ***rac/meso*-2** and ***rac/meso*-3** have been tested for their activity in the polymerization of ethylene and

propylene. These compounds do not polymerize propene, but are very active in ethene polymerization, producing HDPE.

Experimental Section

General Considerations. All organometallic manipulations were performed under an atmosphere of N₂ using standard Schlenk line techniques or an MBraun UNILab glovebox, unless stated otherwise. All organic reactions were carried out under air unless stated otherwise. Solvents used were dried by either reflux over sodium-benzophenone diketyl (THF) or passage through activated alumina (hexane, Et₂O, toluene, CH₂Cl₂) using an MBraun SPS-800 solvent system. Solvents were stored in dried glass ampules, thoroughly degassed by passage of a stream of N₂ gas through the liquid, and tested with a standard sodium benzophenone–THF solution before use. Deuterated solvents for NMR spectroscopy of oxygen- or moisture-sensitive materials were treated as follows: C₆D₆ was freeze–pump–thaw degassed and dried over a K mirror; d₅-pyridine and CDCl₃ were dried by reflux over calcium hydride and purified by trap-to-trap distillation; and CD₂Cl₂ was dried over 3 Å molecular sieves.

¹H and ¹³C NMR spectroscopy were performed using a Varian 300 MHz spectrometer and recorded at 300 K unless stated otherwise. ¹H and ¹³C NMR spectra were referenced via the residual protio solvent peak. Oxygen- or moisture-sensitive samples were prepared using dried and degassed solvents under an inert atmosphere in a glovebox and were sealed in Wilmad 5 mm 505-PS-7 tubes fitted with Young's-type concentric stop-cocks.

Mass spectra were obtained using a Bruker FT-ICR-MS Apex III spectrometer. Elemental microanalyses were conducted by Stephen Boyer at London Metropolitan University.

For single-crystal X-ray diffraction in each case, a typical crystal was mounted on a glass fiber using the oil drop technique, with perfluoropolyether oil, and cooled rapidly to 150 K in a stream of N₂ using an Oxford Cryosystems Cryostream.⁴³ Diffraction data were measured using an Enraf-Nonius KapapaCCD diffractometer (graphite-monochromated Mo K α radiation, λ = 0.71073 Å). Series of ω -scans were generally performed to provide sufficient data in each case to a maximum resolution of 0.77 Å. Data collection and cell refinement were carried out using DENZO-SMN.⁴⁴ Intensity data were processed and corrected for absorption effects by the multiscan method, based on multiple scans of identical and Laue equivalent reflections using SCALEPACK (within DENZO-SMN).

(43) Cosier, J.; Glazer, A. M. *J. Appl. Crystallogr.* **1986**, *19*, 105–197.

(44) Processing of X-ray Diffraction Data Collected in Oscillation Mode; Otwinowski, Z.; Minor, W., Eds.; Academic Press: New York, 1997; Vol. 276.

(45) Altomare, A.; Cascarano, G.; Giacovazzo, C.; Guagliardi, A.; Burla, M. C.; Polidori, G.; Camalli, M. *J. Appl. Crystallogr.* **1994**, *27*, 435.

Structure solution was carried out with direct methods using the program SIR92⁴⁵ within the CRYSTALS software suite.⁴⁶ In general, coordinates and anisotropic displacement parameters of all non-hydrogen atoms were refined freely except where this was not possible due to the presence of disorder (i.e., toluene of crystallization in **meso-2**). Hydrogen atoms were generally visible in the difference map and were treated in the usual manner.⁴⁷ Information on the calculation of derived parameters (using Mercury⁴⁸ and CrystalMaker⁴⁹) is included as Supporting Information. Refinement details are also available in the Supporting Information (CIF). These data (excluding structure factors) have also been deposited with the Cambridge Crystallographic Data Centre; copies can be obtained free of charge via www.ccdc.cam.ac.uk/data_request/cif.

Electrochemical experiments were performed in anhydrous CH_2Cl_2 or THF containing $0.1 \text{ mol}^{-1} [\text{N}^{\text{t}}\text{Bu}_4]\text{[PF}_6]$ as supporting electrolyte, using a Princeton Applied Research VersaSTAT 3 potentiostat controlled by a PC running V3-Studio software. Cyclic voltammetric and square-wave experiments were performed using a three-electrode configuration with a N_2 inlet/outlet bubbler connected to an external oil bubbler and a side-neck fitted with a rubber septum for addition of the samples (G. Glass, Australia). The working electrode used was a Pt disk BASi MF-2013 of 1.6 mm diameter, the counter electrode was a Pt wire, and a Ag wire was the pseudoreference electrode. The electrodes were polished prior to each use. Before each sample was run, the empty cell was thoroughly purged with N_2 , the electrolyte solution thoroughly degassed with N_2 , and a background scan of the solvent window recorded. The sample was dissolved in a small amount of electrolyte, transferred via syringe into the cell, and further degassed. After recording the CV traces, Cp_2Fe was added as an internal reference and acquisition of the voltammograms repeated. The Ag wire pseudoreference electrode was calibrated to the $\text{Cp}_2\text{Fe}/\text{Cp}_2\text{Fe}^+$ couple at +0.46 V vs the saturated calomel electrode (SCE) in CH_2Cl_2 and +0.56 V in THF vs SCE, and all potentials are reported vs SCE. A number of different scan rates were used, and measurements were performed under an inert N_2 atmosphere. Thermodynamic half-potentials were obtained by square-wave voltammetry, and reversibility of the redox process was tested by a plot of the maximum anodic (or minimum cathodic) peak current against the square root of the scan rate, giving a straight line in the reversible cases. Comparison of the anodic to cathodic potential difference with that of the internal Cp_2Fe reference was used to confirm the number of electrons of each redox process.

Polymerization trials and differential scanning calorimetry experiments were run by INEOS Polyolefins at the Neder-Over-Hembeek (NOH) Technology Center. For ethylene polymerization the catalyst precursors (typically, 1.17 mg of catalyst; ca. $2 \mu\text{mol M}$) were dissolved in toluene with half the MMAO activator added in this solution (5000 equivalents vs metal), and the other half was added to the 5 L steel autoclaves. The reactions were run for 30–60 min under 10 bar of ethene. The autoclave was thermostatically controlled to 70 °C. High-temperature gel permeation chromatography was performed using a Polymer Laboratories GPC220 instrument, with one PLgel Olexis guard plus two Olexis 30 cm × 13 μm columns. The solvent used was 1,2,4-trichlorobenzene with antioxidant, at a nominal flow rate of 1.0 mL min^{-1} and nominal temperature of 160 °C. Refractive index and Viscotek differential

pressure detectors were used. The data were collected and analyzed using Polymer Laboratories “Cirrus” software. A single solution of each sample was prepared by adding 15 mL of solvent to 15 mg of sample and heating at 190 °C for 20 min, with shaking to dissolve. The sample solutions were filtered through a glass-fiber filter, and part of the filtered solutions were then transferred to glass sample vials. After an initial delay of 30 min in a heated sample compartment to allow the sample to equilibrate thermally, injection of part of the contents of each vial was carried out automatically. The samples appeared to be completely soluble, and there were no problems with either the filtration or the chromatography of the solutions. The GPC system was calibrated with Polymer Laboratories polystyrene calibrants. The calibration was carried out in such a manner that combined GPC–viscosity could be used to give “true” molecular weight data and conventional GPC could also be applied. For the conventional GPC results, the system is calibrated with linear polyethylene or linear polypropylene. This correction has previously been shown to give good estimates of the true molecular weights for the linear polymers.

For the GPC–viscosity approach, the system is still calibrated using polystyrene, but the use of the refractive index (concentration) and differential pressure (viscosity) detector responses, together with accurate knowledge of the polymer solution concentration, allows computation of “true” molecular weight data without applying any correction. This approach also gives intrinsic viscosity data that allows comparison of long chain branching. Although this approach does give “true” molecular weight data, some parameters are adjusted to ensure a good match for a known material, and the approach used to obtain the polymer sample concentration can be important. For this work, the differential refractive index (dn/dc) for the polyethylene/solvent combination was assumed and the concentration back-calculated from the refractive index detector response. If samples were not simply polyethylene, errors would be introduced due to a change in dn/dc . The differential pressure (viscosity) detector response is a function of concentration and intrinsic viscosity (effective molecular weight), and the response to the propylene oligomer was too low for the application of the GPC–viscosity approach to be sensible.

- (46) Betteridge, P. W.; Carruthers, J. R.; Cooper, R. I.; Prout, K.; Watkin, D. *J. Appl. Crystallogr.* **2003**, *36*, 1487.
- (47) Cooper, R. I.; Thompson, A. L.; Watkin, D. *J. Appl. Crystallogr.* **2010**, *43*, 1100–1107.
- (48) Macrae, C. F.; Bruno, I. J.; Chisholm, J. A.; Edgington, P. R.; McCabe, P.; Pidcock, E.; Rodriguez-Monge, L.; Taylor, R.; van de Streek, J.; Wood, P. A. *J. Appl. Crystallogr.* **2008**, *41*, 466–470.
- (49) *Crystalmaker* ver. 8.2; Crystalmaker Software Ltd: Oxford, UK.
- (50) Soloveichik, G. L.; Arkhireeva, T. M.; Bel'skii, V. K.; Bulychev, B. M. *Metalloorg. Khim.* **1988**, *1*, 226.
- (51) Bohme, U.; Rittmeister, B. CSD Private Communication, **1998**.
- (52) Zachmanoglou, C. E.; Doocrat, A.; Bridgewater, B. M.; Parkin, G.; Brandow, C. G.; Bercaw, J. E.; Jardine, C. N.; Lyall, M.; Green, J. C.; Keister, J. B. *J. Am. Chem. Soc.* **2002**, *124*, 9525–9546.
- (53) Wochner, F.; Zsolnai, L.; Huttner, G.; Brintzinger, H. H. *J. Organomet. Chem.* **1985**, *288*, 69–77.
- (54) Repo, T.; Klinga, M.; Mutikainen, I.; Su, Y.; Leskelä, M.; Polamo, M. *Acta Chem. Scand.* **1996**, *50*, 1116–1120.
- (55) LoCoco, M. D.; Jordan, R. F. *J. Am. Chem. Soc.* **2004**, *126*, 13918–13919.
- (56) Piemontesi, F.; Camurati, I.; Resconi, L.; Balboni, D.; Sironi, A.; Moret, M.; Zeigler, R.; Piccolrovazza, N. *Organometallics* **1995**, *14*, 1256–1266.
- (57) Collins, S.; Kuntz, B. A.; Taylor, N. J.; Ward, D. G. *J. Organomet. Chem.* **1988**, *342*, 21–29.
- (58) Collins, S.; Gauthier, W. J.; Holden, D. A.; Kuntz, B. A.; Taylor, N. J.; Ward, D. G. *Organometallics* **1991**, *10*, 2061–2068.
- (59) Resconi, L.; Piemontesi, F.; Camurati, I.; Balboni, D.; Sironi, A.; Moret, M.; Rychlicki, H.; Zeigler, R. *Organometallics* **1996**, *15*, 5046–5059.
- (60) Kaminsky, W.; Rabe, O.; Schauwienold, A. M.; Schupfner, G. U.; Hanss, J.; Kopf, J. *J. Organomet. Chem.* **1995**, *497*, 181–193.
- (61) Bruce, M. D.; Coates, G. W.; Hauptman, E.; Waymouth, R. M.; Ziller, J. W. *J. Am. Chem. Soc.* **1997**, *119*, 11174–11182.
- (62) Bazhenova, T. A.; Antipin, M. Y.; Babkina, O. N.; Bravaya, N. M.; Lyssenko, K. A.; Strelets, V. V. *Russ. Chem. Bull.* **1997**, *46*, 2048–2052.
- (63) Ewen, J. A.; Haspeslach, L.; Atwood, J. L.; Zhang, H. *J. Am. Chem. Soc.* **1987**, *109*, 6544–6545.
- (64) Loukova, G. V.; Strelets, V. V. *J. Organomet. Chem.* **2000**, *606*, 203–206.

The synthesis of 2,3,4,5,6,7-hexamethyl-1-methyleneindene, $C_{16}H_{20}$, has been reported by us previously.⁵

Preparation of Ethylenebis(hexamethylindenyl), EBI*Li₂·THF_{0.38}, 1. Li (0.13 g, 1.86×10^{-2} mol) and naphthalene (2.56 g, 2.00×10^{-2} mol) were stirred in THF, forming a green solution after 3 h, which still contained Li and so was stirred for a further 15 h. $C_{16}H_{20}$ (3.69 g, 1.74×10^{-2} mol) was dissolved in THF, giving a bright yellow solution, which was added to the dark green $C_{10}H_8Li$ mixture at -78°C . The reaction mixture was stirred at -78°C for 30 min, then allowed to warm to room temperature with stirring. A precipitate formed after 2 h, and after a further 3 h the solvent was removed under vacuum from the yellow-green mixture. The residue was washed with Et₂O and dried to yield an off-white powder. Yield: 3.78 g, 93%. Analysis by NMR spectroscopy showed this solid to be of the formula EBI*Li₂·THF_{0.38}. ¹H NMR (*d*₅-pyridine): δ 2.42, 2.45, 2.62, 2.89, 2.91, 3.06 (all s, 6H, Me), 3.78 (s, 4H, C₂H₄). ¹³C NMR (*d*₅-pyridine): δ 13.8, 16.3, 17.3, 17.4, 18.7, 19.2 (Me), 36.4 (C₂H₄), 97.8, 105.6, 119.1, 119.4, 123.5, 123.6, 124.8, 126.8, 128.8 (ring Cs).

Preparation of *rac*- and *meso*-EBI*ZrCl₂, 2. Compound **1** (0.35 g, 7.51×10^{-4} mol) was slurried in toluene and cooled to -78°C . To this orange-red slurry was added a white slurry of ZrCl₄·THF₂ (0.28 g, 7.51×10^{-4} mol) in toluene. No immediate change was observed, and the reaction mixture was allowed to warm to room temperature with stirring. After stirring for a further 15 h, the red-brown reaction mixture was filtered, affording a red-orange solution. The residues were extracted with CH₂Cl₂ and the extracts combined. Removal of the solvent under vacuum gave a red-orange solid, which was washed with -78°C hexane. The resultant residue was extracted with room-temperature hexane to give a red-orange solid and yellow-orange solution. NMR analysis of this solid showed it to be an approximately 1:0.8 *rac/meso* mix. The solvent was removed under vacuum from the yellow-orange solution to give an orange solid; NMR analysis of this solid indicated it to be mainly composed of **meso-2** with a tiny proportion of impurities including the *rac*-isomer.

The *rac/meso* mix was extracted and filtered with CH₂Cl₂ to afford a red solution, which was layered with hexane. The yellow supernatant was decanted via cannula, leaving an orange solid, shown by NMR analysis to be pure **rac-2**. The supernatant was reduced under vacuum to an orange solid, a more *meso*-enriched mixture of isomers, and washed with 60°C hexane, leaving pure *rac*-isomer. The orange-yellow solution was again reduced to an isomeric solid mix, extracted with 60°C hexane, and cooled to -80°C , depositing a final crop of **rac-2**. Crystals of **rac-2** suitable for X-ray diffraction were grown as pale orange plates by layering a CD₂Cl₂ solution of the sample with Et₂O.

The predominantly *meso* extracts were further extracted with 60°C hexane and filtered, reduced to a minimum volume, and cooled slowly to -35°C . Orange needles of pure **meso-2** suitable for X-ray diffraction were collected and washed with -78°C hexane. Yield: 0.060 g, 0.028 g, total 20%. HRMS (EI): calcd 584.1554, found 584.1567. Anal. Calcd for $C_{32}H_{40}ZrCl_2$: C, 65.50; H, 6.87. Found: C, 65.44; H, 6.79.

rac-EBI*ZrCl₂ (**rac-2**). ¹H NMR (C₆D₆): δ 1.78, 2.11, 2.22, 2.43, 2.46, 2.56 (all s, 6H, Me), 3.22–3.40, 3.70–3.88 (m, 4H, C₂H₄). (CDCl₃): δ 1.84, 2.23, 2.29, 2.33, 2.40, 2.79 (all s, 6H, Me), 3.65–3.81, 4.02–4.18 (m, 4H, C₂H₄). (CD₂Cl₂): δ 1.84, 2.24, 2.29, 2.31, 2.37, 2.80 (all s, 6H, Me), 4.03–4.22, 3.63–3.82 (m, 4H, C₂H₄). ¹³C NMR (CD₂Cl₂): δ 12.0, 15.9, 16.6, 16.9, 17.7, 18.0 (Me), 32.9 (C₂H₄), 116.0, 118.8, 123.6, 125.2, 126.4, 128.8, 129.5, 130.7, 134.6 (ring Cs).

meso-EBI*ZrCl₂ (**meso-2**). ¹H NMR (C₆D₆): δ 1.85, 1.99, 2.01, 2.39, 2.51, 2.52 (all s, 6H, Me), 3.20–3.34, 3.74–3.88 (m, 4H, C₂H₄). (CDCl₃): δ 2.12, 2.13, 2.16, 2.32, 2.45, 2.60 (all s, 6H, Me), 3.63–3.80, 4.07–4.24 (m, 4H, C₂H₄). (CD₂Cl₂): 2.13 (s, 12H, Me), 2.17, 2.29, 2.43, 2.61 (all s, 6H, Me), 3.64–3.82, 4.08–4.26 (m, 4H, C₂H₄). ¹³C NMR (C₆D₆): δ 13.3, 15.7, 16.5, 16.9, 17.6, 17.7 (Me), 31.4 (C₂H₄), 106.7, 114.0, 121.5, 127.0,

127.3, 129.0, 130.7, 133.0, 134.1 (ring Cs). (CDCl₃): δ 13.5, 15.4, 16.5, 16.8, 17.4, 17.4 (Me), 31.3 (C₂H₄), 104.1, 114.2, 121.6, 126.3, 126.8, 129.5, 130.2, 133.0, 134.3 (ring Cs).

Synthesis of *rac*- and *meso*-EBI*HfCl₂, 3. To an orange-red slurry of EBI*Li₂·THF_{0.38} (0.35 g, 7.51×10^{-4} mol) in toluene at -78°C was added a white slurry of HfCl₄·THF₂ (0.35 g, 7.51×10^{-4} mol) in toluene. The reaction mixture was allowed to warm to room temperature with stirring, with no observed change. After stirring for 15 h, an aliquot was taken and NMR analysis showed a 1.7:1 mix of *meso/rac*-isomers. The yellow-brown reaction mixture was filtered, and the remaining solid extracted with toluene and combined to give an orange-brown solution. Removal of the solvent under vacuum afforded a yellow-orange solid, which was extracted with hot hexane, giving a bright yellow solution and buff powder, shown by NMR analysis to be a 1:1 mix of *rac/meso*-isomers. Removal of the solvent under vacuum from the bright yellow solution left a bright yellow solid, consisting by NMR analysis of predominantly **meso-3** with a small amount of the *rac*-isomer, and was purified to the pure *meso* form by extraction with room-temperature hexane and filtration.

The buff *rac/meso* mix was extracted with hot hexane and filtered, giving a yellow solution, removal of the solvent under vacuum from which gave a solid consisting of mainly the *meso*-isomer with a small impurity including the *rac* form. Another extraction of this solid with 60°C hexane afforded a yellow solution plus a yellow solid. This yellow solid was dissolved in CH₂Cl₂, reduced to a minimum volume, and layered with hexane. A light yellow solid precipitated, and removal of the supernatant via cannula left pure **rac-3**. The second yellow hexane extraction was reduced to a minimum volume and cooled to -35°C , whereupon a bright yellow solid crop of **meso-3** was collected and washed with -78°C hexane.

Single crystals of the *meso* form suitable for analysis by X-ray diffraction were grown as pale yellow plates by the cooling of a saturated isomerically pure hexane solution of **meso-3** to -35°C . X-ray diffraction quality crystals of the *rac*-isomer were obtained as pale yellow needles by the slow evaporation of an NMR pure C₆D₆ solution of **rac-3**. Yield: 0.095 g, 0.057 g, total 30%. MS (EI): calcd 674.1957, found 674.1969. Anal. Calcd for $C_{32}H_{40}HfCl_2$: C, 57.02; H, 5.98. Found: C, 57.08; H, 6.06.

rac-3. ¹H NMR (C₆D₆): δ 1.82, 2.12, 2.25, 2.46, 2.48, 2.55 (all s, 6H, Me), 3.43–3.52, 3.66–3.75 (m, 4H, C₂H₄). (CDCl₃): δ 1.88, 2.24, 2.31 (all s, 6H, Me), 2.38 (s, 12H, Me), 2.77 (s, 6H, Me), 3.83–3.94, 3.95–4.06 (m, 4H, C₂H₄). (CD₂Cl₂): δ 1.89, 2.26, 2.32, 2.34, 2.36, 2.79 (all s, 6H, Me), 3.85–3.94, 3.98–4.07 (m, 4H, C₂H₄). ¹³C NMR (CD₂Cl₂): δ 11.5, 15.7, 16.2, 16.5, 16.8, 17.7 (Me), 32.2 (C₂H₄), ring Cs not visible.

meso-3. ¹H NMR (C₆D₆): δ 1.90, 2.01, 2.03, 2.39, 2.49, 2.57 (all s, 6H, Me), 3.23–3.40, 3.78–3.95 (m, 4H, C₂H₄). (CDCl₃): δ 2.13, 2.15, 2.22, 2.32, 2.51, 2.57 (all s, 6H, Me), 3.68–3.84, 4.11–4.27 (m, 4H, C₂H₄). ¹³C NMR (C₆D₆): δ 13.2, 15.5, 16.4, 16.8, 17.6, 17.7 (Me), 30.7 (C₂H₄), 110.8, 119.1, 125.3, 126.2, 126.3, 127.4, 130.5, 132.7, 133.8 (ring Cs). (CDCl₃): δ 13.7, 15.2, 16.4, 16.7, 17.4, 17.4 (Me), 30.6 (C₂H₄), 110.9, 119.2, 124.9, 125.4, 126.5, 127.9, 130.0, 132.8, 134.0 (ring Cs).

Synthesis of *rac*- and *meso*-EBI*ZrMe₂, 4. A sample of **rac-2** was suspended in Et₂O and cooled to -78°C . To this orange suspension was added an excess of 1.56 M MeLi·LiBr in Et₂O, and the reaction mixture allowed to warm to room temperature. The initial orange suspension became a yellow solution and was stirred for a further 2 h. Removal of the solvent under vacuum, extraction with hexane, and removal of the volatiles afforded a light orange-yellow solid, shown by NMR analysis to be **meso-4**. The use of low-halide MeLi in Et₂O with **rac-2** was found to yield **rac-4**. A similar procedure was followed with **meso-2** and 1.56 M MeLi·LiBr in Et₂O, affording **meso-4**.

rac-4. ¹H NMR (C₆D₆): δ -0.99 (s, 6H, Zr-Me), 1.69, 2.12, 2.22, 2.41, 2.49, 2.51 (all s, 6H, Me), 3.12–3.29, 3.41–3.58 (m, 4H, C₂H₄).

meso-4. ^1H NMR (C_6D_6): δ –2.33, –0.20 (both s, 3H, Zr-Me), 1.77, 2.04, 2.07, 2.41, 2.42, 2.48 (all s, 6H, Me), 2.95–3.12, 3.53–3.70 (m, 4H, C_2H_4). (CDCl_3): δ –2.88, –0.62 (both s, 3H, Zr-Me), 2.03, 2.11, 2.14, 2.38, 2.39, 2.48 (all s, 6H, Me), 3.23–3.38, 3.68–3.83 (m, 4H, C_2H_4).

Acknowledgment. We thank ESPRC for financial support and INEOS Polyolefins, Neder-Over-Hembeek

(NOH) Technology Center, Belgium, for the polymerization studies.

Supporting Information Available: Crystallographic data for **rac-2**, **meso-2**, **rac-3**, and **meso-3** (CIF), tables of bond lengths and angles, details for calculating derived parameters, and GPC–viscosity data for the polyethene samples. This material is available free of charge via the Internet at <http://pubs.acs.org>.